One-demensional Simulation of Drop Breakup in Inkjet

H. Jiang, H. Tan

Washington State University Vancouver, ENCS
14204 NE Salmon Creek Ave, Vancouver, WA, 98686, USA, hua.tan@wsu.edu

ABSTRACT

In this study, we use a simplified 1D slender-jet analysis based on the lubrication approximation to study the drop breakup in inkjet. In this model, the free-surface is represented by a shape function so that the full Naiver-Stokes equation can be linearized into a set of simple partial different equations (PDEs). Then the discrete PDEs are solved by method of lines (MOL) in a moving uniform staggered mesh in Lagrangian coordinates. The MATLAB is used to implement the algorithm and simulation. Finally, we validate the model using 2D computational fluid dynamics (CFD) simulations and established data from previous paper. The research demonstrate that the proposed model enables rapid parametric analysis of drop breakup and satellite droplets formation as a function of nozzle dimensions, driving pulse and fluid properties.

Keywords: Plateau-Rayleigh instability, method of lines, drop-on-demand inkjet, drop breakup

1 INTRODUCTION

Despite the traditional appliction of inkjet technology in printing industry is facing increasing challenge from electronic media and idea of "paperless world", the technology becomes even more prosperous in last decade with a wide range of noval applications in manufacturing and research proliferating. Because of its ability to precisely deliver pico-volume of liquid at high speed and low cost, inkjet technology attracts attention from additive manufacturing [1], electronic device prototyping [2], tissue engineering [3], pharmaceutics [4] and spray cooling of electronics [5]. Generally speaking, inkjet devices are classified as two kinds: countinuous inkjet (CIJ) and drop-on-demand (DoD) inkjet which are distinguished by the form of ejected liquid. The CIJ device eject a continuous stream of liquid, whereas the DoD device eject drops at a regular interval controlled by electronic signals.

When the liquid is ejected from the DoD inkjet device, it undergoes a series of physical events: 1. the drop emerging from the nozzle due to actuation; 2. the drop pinching off from the nozzle; 3. the drop breaking up into main droplet followed by multiple satellite droplets. Satellite droplets often cause detrimental effect on printing quality, because they tend to scatter on the substrate. Therefore, fundamental understanding of breakup of droplet ejection is vital to various applications of the inkjet technology.

Drop breakup in inkjet is determined by the Plateau-Rayleigh (PR) instability which explains why and how a stream of fluid breaks up into smaller packets with the same volume but less surface area. The explanation begins with the existence of perturbations in the the stream. Due to surface tension, the perturbation leads to an inhomogeneous distribution of pressure in liquid stream which squeezes liquid out of area with larger mean curvature and eventually results in a breakup. If the perturbation are decomposed into sinusoidal wave components, the wavelength of the fastest growing component is about nine times of the orifice radius and this wave will dominate the shape evolution of liquid [6]. However, it is not easy to apply PR instability to inkjet process directly. Multiphase CFD simulations have been used to study the droplet ejection in inkjet technology.

In the past, we have successfully developed a 3D CFD code based on finite-volume method (FVM) to model the drop ejection process from inkjet print-heads [7-8]. Although the full-scale CFD simulations can reveal the physical details in drop breakup, it is not suitable for optimizing device design owing to high computational costs.

In this paper, we use the simplified 1D slender-jet analysis based on the lubrication approximation to study the drop breakup in inkjet [9]. In this model, the free-surface (liquid-air interface) is represented by a shape function so that the full Naiver-Stokes equation can be linearized into a set of simple PDEs of motion. The discrete PDEs are solved by MOL in which PDEs are transformed into a system of ordinary differential equations (ODEs). Because of the motion of drops and to circumvent frequent remeshing, the arbitrary Lagrangian-Eulerian method [9] is applied and surface evolution is tracked by a moving uniform staggered mesh in Lagrangian coordinates. The MATLAB is used to implement the algorithm and simulation.

First we validate the breakup time of an infinite microthread of fluid. Then momentum conservation is tested by a sphere drop with initial velocity. After that, mass conservation and capillary time are tested by a short finite length filament. Finally, we compare the shape evolution of a long filament from our 1D model with a 2D FVM CFD simulation. We find that all of our results have good agreement with previuosly published data and 2D simulations.

2 ALGORITHM

In this section we present how to reduce the govering equation into two coupled PDEs of motion for an axisymmetric incompressible Newtonian fluid and give explanation about our numerical method.

We neglect gravity and suppose dynamic viscosity, surface tension, density and shape function of fluid as μ, σ, ρ and h(z,t), respectively. The governing equation are:
Navier-Stokes eq.

$$\rho\left(\frac{\partial v_r}{\partial t}+v_r\frac{\partial v_r}{\partial r}+v_z\frac{\partial v_r}{\partial z}\right)=-\frac{\partial p}{\partial r}+\mu\left[\frac{1}{r}\frac{\partial}{\partial r}\left(r\frac{\partial v_r}{\partial r}\right)+\frac{\partial^2 v_r}{\partial z^2}-\frac{u_r}{r^2}\right] \quad (1)$$

$$\rho\left(\frac{\partial v_z}{\partial t}+v_r\frac{\partial v_z}{\partial r}+v_z\frac{\partial v_z}{\partial z}\right)=-\frac{\partial p}{\partial z}+\mu\left[\frac{1}{r}\frac{\partial}{\partial r}\left(r\frac{\partial v_z}{\partial r}\right)+\frac{\partial^2 v_z}{\partial z^2}\right] \quad (2)$$

Continuity eq.

$$\frac{1}{r}\frac{\partial v_r}{\partial r}+\frac{\partial v_z}{\partial z}=0 \quad (3)$$

The shear stress along interface is neglected, which gives the first boundary condition (BC):

$$\vec{n}\cdot\mathrm{T}\cdot\vec{t}=0\big|_{r=h} \quad (4)$$

The stress balance in normal direction of interface gives the second BC:

$$\vec{n}\cdot\mathrm{T}\cdot\vec{n}=-\sigma\left(\frac{1}{R_1}+\frac{1}{R_2}\right)\Bigg|_{r=h} \quad (5)$$

In equation (4) and (5), T is the stress tensor in fluid, $\vec{n}$ and $\vec{t}$ are unit vectors normal and tangential to the interface, and R_1 and R_2 are the principal radii of curvature. Apparently, the right-hand side (RHS) of (4) is Young-Laplace equation which represents the capillary pressure difference across the interface. In detail, (4) and (5) give:

$$\frac{\mu}{\left(1+h'^2\right)}\left[2h'\left(\frac{\partial v_r}{\partial r}-\frac{\partial v_z}{\partial z}\right)-\left(1-h'^2\right)\left(\frac{\partial v_r}{\partial z}+\frac{\partial v_z}{\partial r}\right)\right]=0\big|_{r=h} \quad (6)$$

$$\mathrm{p}+\frac{2\mu}{\left(2+h'^2\right)}\left[h'\left(\frac{\partial v_z}{\partial r}+\frac{\partial v_r}{\partial z}\right)-\frac{\partial v_r}{\partial r}-h'^2\frac{\partial v_z}{\partial z}\right]=-\sigma\left(\frac{1}{R_1}+\frac{1}{R_2}\right)\Bigg|_{r=h} \quad (7)$$

$$\frac{1}{R_1}+\frac{1}{R_2}=\frac{1}{h\left(1+h'^2\right)^{1/2}}-\frac{h''}{\left(1+h'^2\right)^{3/2}} \quad (8)$$

where the prime refers to differentiation with respect to z.

Because the radial velocity field at interface is exactly the change rate of shape, it gives the thrid BC:

$$\frac{Dh}{Dt}=\frac{\partial h}{\partial t}+v_z h'=v_r\big|_{r=h} \quad (9)$$

Note that the object of our model is a slender column of liquid whose axial scale is much larger than the radial scale, thus lubrication approximation can be applied. In this approximation, radial inertia is neglected, and axial velocity and pressure are assumed to be uniform in radial direction, so the Taylor series of v_z and p can be just in regard to r:

$$v_z(r,z,t)=v_0(z,t)+v_2(z,t)r^2+\ldots \quad (10)$$

$$p(r,z,t)=p_0(z,t)+p_2(z,t)r^2+\ldots \quad (11)$$

From continuity equation (3) and (10), we obtain:

$$v_r(r,z,t)=-\frac{r}{2}\frac{\partial v_0(z,t)}{\partial z}-\frac{r^3}{4}\frac{\partial v_2(z,t)}{\partial z}+\ldots \quad (12)$$

After pluging (10)-(12) into (1), (2) and (6)-(9), and solving these equations to lowest order in r, we finally get two coupled PDEs of motion:

$$\frac{\partial v}{\partial t}=-v\frac{\partial v}{\partial z}-\frac{\sigma}{\rho}\frac{\partial H}{\partial z}+\frac{3\mu}{\rho h^2}\frac{\partial}{\partial z}\left(h^2\frac{\partial v}{\partial z}\right) \quad (13)$$

$$\frac{\partial h^2}{\partial t}=\frac{\partial}{\partial z}\left(h^2 v\right) \quad (14)$$

$$\mathrm{H}=\frac{1}{h\left(1+h'^2\right)^{1/2}}-\frac{h''}{\left(1+h'^2\right)^{3/2}} \quad (15)$$

in which H is double of mean curvature which determines capillary pressure.

Previous analysis is all based on Euler coordinates and not compatible with a moving boundary, therefore the equation of motion need to be modified to fit to a Lagrangian coordinates. In the pure Lagrangian method, nodes move with the fluid velocity, which often causes severe distortion of mesh after a period of time. As a result, frequent checking of mesh quality and remeshing increases the computional cost. To avoid this disadvantage, we use the arbitrary Lagragian-Euler method to ensure that nodes are always evenly distributed between two ends of liquid filament.

First, we map a fixed computation space x to the moving physical space *z* [9]:

$$z(x,t)=xL(t)+B(t) \quad \left(z\in[B,B+L],\ x\in[0,1]\right) \quad (16)$$

where *B* is the z coordinate of beginning point of liquid, *L* is the length of liquid in physical space. Because of the linear relationship, nodes in physical space always have the same distribution as computation space.

Now we calculate the total time derivative in computation space with chain rule. Let's operate on a scalar field $\phi(z,t)$:

$$\frac{d\phi}{dt}=\frac{\partial\phi}{\partial t}+\frac{\partial\phi}{\partial z}\frac{dz}{dt}=\frac{\partial\phi}{\partial t}+\left(x\dot{L}+\dot{B}\right)\frac{\partial\phi}{\partial z} \quad (17)$$

in which $\dot{B}$ is the the velocity of beginning node $v_{begin,}$ and $\dot{L}$ is the contraction/relaxation rate of liquid v_{end}-v_{begin} .

Substituting ϕ with v and h, and inserting them into (13) and (14), we get the modified equation of motion in Lagrangian cooridnate. In addition, for completeness, equation (15) is writed here again.

$$\frac{dv}{dt} = (x\dot{L} + \dot{B} - v)\frac{\partial v}{\partial z} - \frac{\sigma}{\rho}\frac{\partial H}{\partial z} + \frac{3\mu}{\rho h^2}\frac{\partial}{\partial z}\left(h^2\frac{\partial v}{\partial z}\right) \tag{18}$$

$$\frac{dh^2}{dt} = (x\dot{L} + \dot{B})\frac{\partial h^2}{\partial z} + \frac{\partial}{\partial z}\left(h^2 v\right) \tag{19}$$

$$\mathrm{H} = \frac{1}{h\left(1+h'^2\right)^{1/2}} - \frac{h''}{\left(1+h'^2\right)^{3/2}} \tag{20}$$

We reiterate that the velocity and height are not tracked by a pure Lagrangian coordinates and the node don't move with fluid velocity. This Lagrangian coordinates is defined by equation (16) and that is why (18) and (19) still retain the advection term.

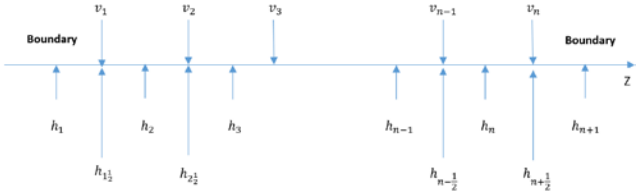

Figure 1: uniform staggered mesh.

Discrete equations of motion (18)-(20) are solved by MOL [10] subject to appropriate BCs and initial conditions (ICs). Specifically, we define a uniform staggered mesh in computational space and use finite difference method to represent all the partial spatial derivative term in RHS of (18)-(20). For example, we apply first order upwind scheme for advection term and second order central difference scheme for the other terms. In this way, (18) and (19) are transformed into two ordinary equations with only partial time derivative of v and h on the left-hand side (LHS). We integrate v in one set of nodes and integrate h and H in the other set of staggered nodes as shown in Figure 1. Ultimately MATLAB ODE sover routine 'ode23t' is used to implement MOL.

3 RESULT

In order to consistently compare our results, we use initial radius r_0 as the length scale and capillary time $t_{cap} = \sqrt{\rho r_0^3/\sigma}$ as the time scale to nondimensionlize (18)-(20). Dimensionless (19)-(20) have the same appearance as before, but (18) is transformed into:

$$\frac{dv}{dt} = (x\dot{L} + \dot{B} - v)\frac{\partial v}{\partial z} - \frac{\partial H}{\partial z} + \frac{3Oh}{h^2}\frac{\partial}{\partial z}\left(h^2\frac{\partial v}{\partial z}\right) \tag{21}$$

where v, t, z, h, $\dot{B}$ and $\dot{L}$ are all dimensionless, and Oh is Ohnesorge number. If the fluid has no initial velocity, Reynolds number can be modified by capillary velocity v_{cap}. Consequently, Reynolds number becomes the inverse of Ohnesorge number.

$$v_{cap} = \frac{r_0}{t_{cap}} = \sqrt{\frac{\sigma}{\rho r_0}} \tag{22}$$

$$\mathrm{Re} = \frac{\rho v_{cap} r_0}{\mu} = \frac{\sqrt{\rho\sigma r_0}}{\mu} = \frac{1}{Oh} \tag{23}$$

Note that fluid with Oh 0.01-0.1 is usually regarded as printable, thus our analysis hereafter are mainly based on this window.

We first validate the breakup time by an infinite microthread of fluid with sinusoidal perturbation. With wavelength λ and amplitude ratio ε, the shape of fluid is described by

$$h(z,0) = r_0\left[1 + \varepsilon\cos\left(\frac{2\pi z}{\lambda}\right)\right] \tag{24}$$

In the same way, we scale wave length by r_0, so the scaled wavenumber becomes $k=2\pi r_0/\lambda$.

	k=0.2	k=0.45	k=0.7	k=0.9
Re=200	25.213	12.911	10.035	14.495
	25.0	12.6	9.7	11.0
	25.036	**12.722**	**9.767**	**11.098**
Re=10	26.683	14.299	11.623	14.83
	27.9	14.3	11.4	14.4
	27.005	**14.306**	**11.480**	**14.523**
Re=0.1	230.6	243.2	311.9	628.2
	227	238	305	634
	234.025	**245.748**	**313.740**	**642.686**

Table 1: Comparison of scaled breakup times (bold font) with Ashgriz's (first row) FEM model and Furlani's 1D model (second row).

By choosing a set of simple parameter of ρ=1g/cm^3, σ=1dyn/cm, r_0=0.2cm and ε=0.05, we acquire scaled breakup times in different k and Re, and compare them with published data from Ashgriz [11] and Furlani [12] in Table1. Obviously, good agreement was achieved. Figure 2 shows the evolution of droplet profile at the breakup moment and post-breakup when k=0.7 and Re=10.

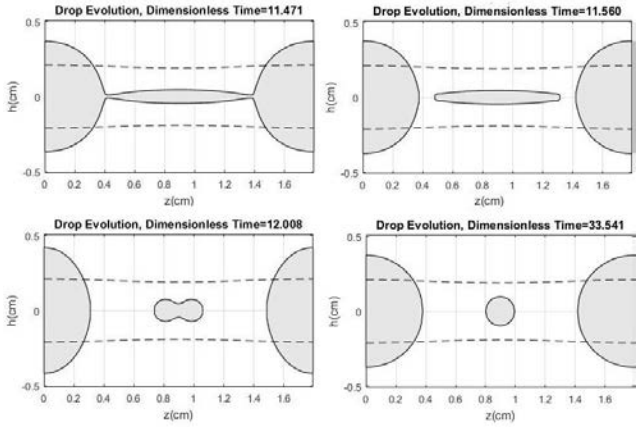

Figure 2: Breakup moment for k=0.7, Re=10, the dash line represents initial shape of fluid.

Next, we perform a calculation on a sphere drop with initial velocity 10 cm/s to test the momentum and the mass conservation. Parameter are given as ρ=1g/cm^3, σ=1dyn/cm, r_0=1cm and μ=0.01P, and results are shown in Figure 3. We can find that except the slightly increase at the first 0.04s, the momentum is well conserved from the simulation. The time variation of momentum is negligible.

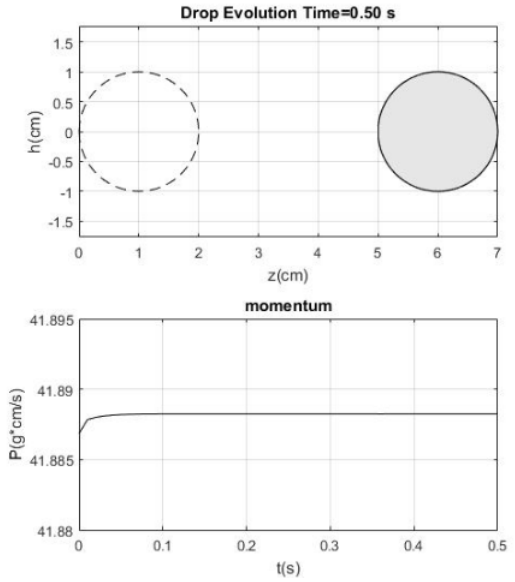

Figure 3: drop position and momentum-time curve.

Lastly, we apply our model to a finite length filament which has a column body and two semisphere ends. If the filament is short, it will contract into a sphere and oscillate several times before getting stable. The parameters are ρ=1g/cm^3, σ=1dyn/cm, r_0=0.2cm, μ=0.045P and L_0=1.8cm The results are plotted in Figure 4. Mass variation is very small less than 0.2%. The time history of horizontal diameter (i.e., the distance between two ends of the filament) reveals the oscillation period of 0.41s which is close to the capillary time 0.44s. The comparion of time history of horizontal diameter between 1D and 2D simulations is shown in Figure 4. It is clear that the result from 1D agrees very well with that from 2D simulation during contracting phase. The 1D model begins to diverge from the 2D model during oscillation stage. It is because that the large vorticity is generated during oscillation, which makes the 1D assumption not valid [13-14].

To look at shape evolution more closely, we do a similar simulation as above, but this time we make the filament much longer and compare it with a 2D FVM simultion. Parameters are ρ=1g/cm^3, σ=1dyn/cm, r_0=1cm, μ=0.1P and L_0=30cm. The camparison is shown in Figure5 in which solid line is from 1D model and dash line is from 2D model. Obviously, The dash line and the solid line are nearly identical to each other.

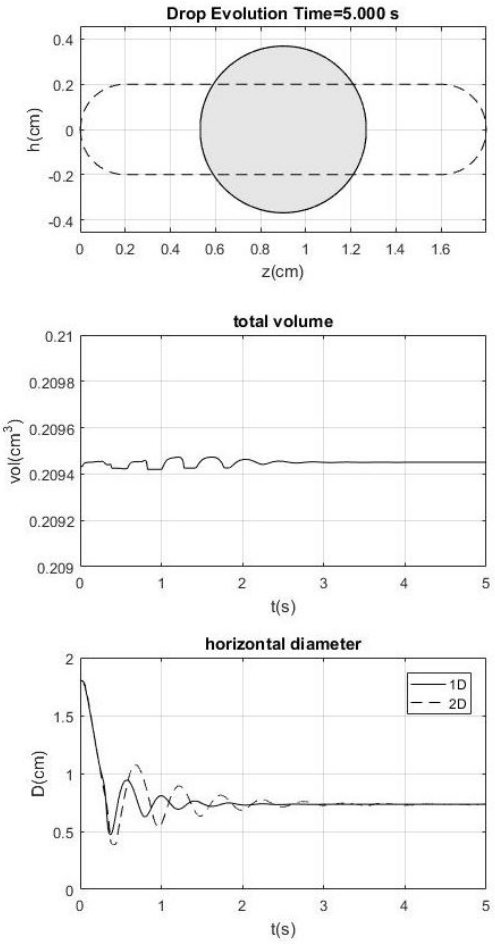

Figure 4: filament contraction, total volume-time curve and horizontal diameter-time curve (oh=0.1).

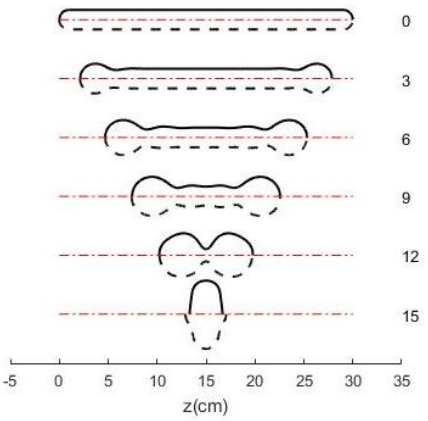

Figure 5: shape evolution of a long filament, solid line is 1D model and dash line is 2D model (oh=0.1).

4 CONCLUSION

We have developed a 1D numerical model to describe drop breakup. The model is based on lubrication approximation and solved by MOL in a moving mesh. The MOL is implemented by a MATLAB ODE solver routine. We validated the model using established data from literature as well as FVM 2D CFD simulation. The research demonstrates that the proposed model enables rapid parametric analysis of drop breakup and satellite droplets formation as a function of nozzle dimensions, driving pulse and fluid properties.

REFERENCES

[1] Thomas, Helen R., Neil Hopkinson, and Poonjolai Erasenthiran. "High speed sintering—continuing research into a new rapid manufacturing process." *Proceedings of 17th SFF Symposium, Austin, TX*. 2006.

[2] Kawahara, Yoshihiro, et al. "Instant inkjet circuits: lab-based inkjet printing to support rapid prototyping of UbiComp devices." *Proceedings of the 2013 ACM international joint conference on Pervasive and ubiquitous computing*. ACM, 2013.

[3] Saunders, Rachel Elizabeth, and Brian Derby. "Inkjet printing biomaterials for tissue engineering: bioprinting." *International Materials Reviews* 59.8 (2014): 430-448.

[4] Daly, Ronan, et al. "Inkjet printing for pharmaceutics–a review of research and manufacturing." *International journal of pharmaceutics* 494.2 (2015): 554-567.

[5] Bash, Cullen E., Chandrakant D. Patel, and Ratnesh K. Sharma. "Inkjet assisted spray cooling of electronics." *ASME 2003 International Electronic Packaging Technical Conference and Exhibition*. American Society of Mechanical Engineers, 2003.

[6] Rayleigh L. "On the capillary phenomena of jets." *Proc. R. Soc. London.* Vol. 29. No. 196-199. 1879

[7] Tan, Hua, et al. "Numerical simulation of droplet ejection of thermal inkjet printheads." *International Journal for Numerical Methods in Fluids* 77.9 (2015): 544-570.

[8] Tan, Hua, An adaptive mesh refinement based flow simulation for free-surfaces in thermal inkjet technology. *International Journal of Multiphase Flow*. 82, 1-16, 2016.

[9] Hanchak, Michael Stephen. *One dimensional model of thermo-capillary driven liquid jet break-up with drop merging*. Diss. University of Dayton, 2009.

[10] Schiesser, William E. *The numerical method of lines: integration of partial differential equations*. Elsevier, 2012.

[11] Ashgriz, N., and Farzad Mashayek. "Temporal analysis of capillary jet breakup." *Journal of Fluid Mechanics* 291 (1995): 163-190.

[12] Furlani, E. P., and M. S. Hanchak. "Nonlinear analysis of the deformation and breakup of viscous microjets using the method of lines." *International Journal for Numerical Methods in Fluids* 65.5 (2011): 563-577.

[13] Notz, Patrick K. and Basaran, Osman A., "Dynamics and breakup of a contracting liquid filament." *Journal of Fluid Mechanics*, 512, 2004, 223-256

[14] Hoepffner, Jerome and Pare, Gounseti, "Recoil of a liquid filament: escape from pinch-off through creation of a vortex ring." *Journal of Fluid Mechanics*, 734, 2013, 183-197.